WELDING RESEARCH

SUPPLEMENT TO THE WELDING JOURNAL, JANUARY, 1985

Sponsored by the American Welding Society and the Welding Research Council

TECHNICAL PAPERS EDITOR: T.P. SCHOONMAKER

Readers are advised that all papers published in the *Welding Journal's* Research Supplement undergo Peer Review before publication for: 1) originality of the contribution; 2) technical value to the welding community; 3) prior publication of the material being reviewed; 4) proper credit to others working in the same area; and 5) justification of the conclusions based on the results.

The names of the more than 160 individuals serving on the AWS Peer Review Panel are published periodically. All are experts in their respective technical areas, and all are volunteers in the program.

Dissolution and Deposit of Base Metal in Dissimilar Metal Brazing

Joints are affected significantly by differences in carbon content of two dissimilar metals brazed together using copper filler metal

BY T. YOSHIDA AND H. OHMURA

ABSTRACT. The study discussed in this paper was performed to investigate solid-liquid interface phenomena in dissimilar metal brazing with Cu filler metal.

In joining Fe with alloying elements such as C, Cr, Co, Ni, W and V to a second base metal, the deposited alloy phase includes components of the second base metal. This phase develops in the braze interface with heating time even though the brazing temperature is kept constant – that is, a "dissolution and deposit of base metal" takes place in all cases.

When alloy steels such as high speed T4 tool steel and Type 304 stainless steel are brazed to low and high carbon steels, dissolution and deposit also take place. Moreover, joint configuration is affected significantly by the difference of carbon (C) content between both base metals regardless of the other alloying elements. When Cu is the filler metal, the lower carbon base metal dissolves in the molten filler metal and, simultaneously, a columnar Fe alloy phase is deposited from the higher C base metal at a constant brazing temperature.

The shear strength of the dissimilar alloy steel joints is enhanced remarkably by linking both base metals with the columnar deposited phase. An exception occurs with stainless steel/high carbon steel joints in that a chromium carbide forms at the high carbon boundary.

Based on a paper presented at the 13th International AWS-WRC Brazing and Soldering Conference held in Kansas City, Missouri, during April 27-29, 1982.

T. YOSHIDA is Professor, Transport Machine Engineering Department, Meijyo University, Nagoya, and H. OHMURA is Research Metallurgist, Nagoya Municipal Industrial Research Institute, Nagoya, Japan.

Introduction

In brazing dissimilar carbon steels with Cu filler metal (Ref. 1), the low carbon steel dissolves in molten Cu. Simultaneously, the dissolved iron deposits as a columnar Fe-Cu-C alloy from the high carbon steel at a constant brazing temperature. This phenomenon has been named "dissolution and deposit of base metal" (Ref. 2). When both base metals are linked with the columnar phase, the shear strength of the brazed joint is increased remarkably .

The dissolution and deposit of base metal has occurred, when certain conditions are satisfied, in various dissimilar metal brazes (Refs. 3-5) without regard to whether the base metal to be joined is pure metal or alloy.

The study reported in this paper undertook to examine the dissolution phenomena and deposits occurring when brazing Fe to various pure metals using Cu filler metal. An objective was to review the mechanisms governing what took place. Furthermore, the shear strengths of the brazed joints for dissimilar alloy steels were investigated.

Experimental Procedure

Brazing tests were conducted utilizing both similar and dissimilar joints involving the following materials:

1. Pure iron (99.65% Fe, 0.013% C).
2. Chromium (99.5% Cr).
3. Nickel (99.9% Ni).
4. Cobalt (99.8% Co).
5. Tungsten (99.9% W).
6. Vanadium (99.7% V).
7. Carbon (C) in the form of graphite.
8. Low carbon steel with 0.11% C.

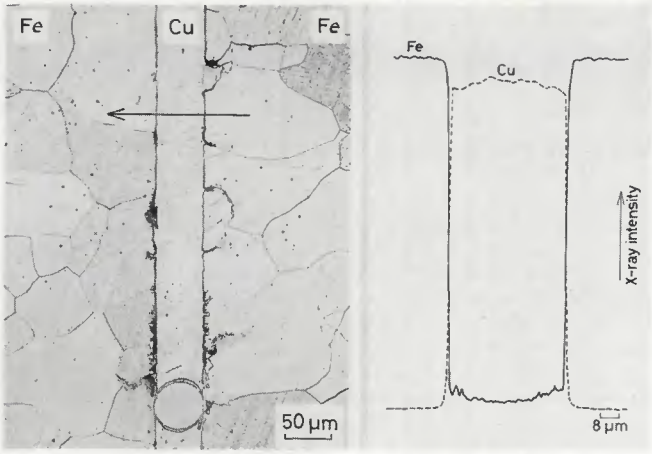

Fig. 1 — Microstructure and EPMA line analysis of Fe-BCu-Fe joint at 50 µm (0.002 in.), brazed at 1125°C (2057°F) for 8 min

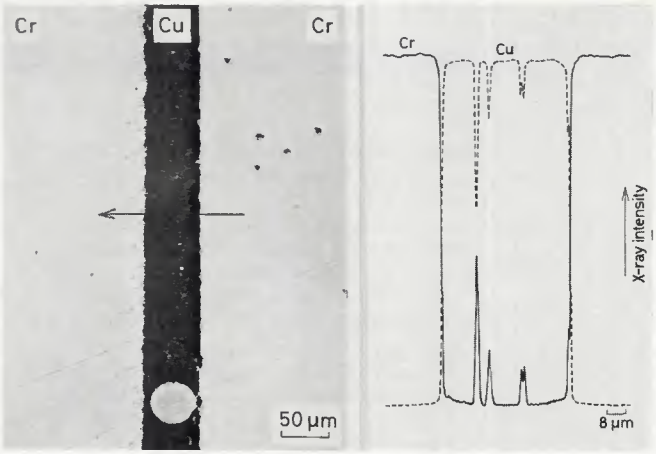

Fig. 2 — Microstructure and EPMA line analysis of Cr-BCu-Cr joint at 50 µm (0.002 in.), brazed at 1150°C (2102°F) for 8 min in Ar

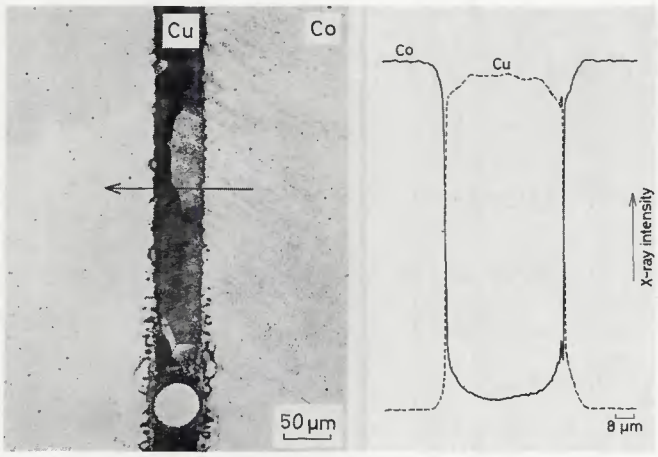

Fig. 3 — Microstructure and EPMA line analysis of Co-8Cu-Co joint at 50 µm (0.002 in.), brazed at 1125°C (2057°F) for 8 min

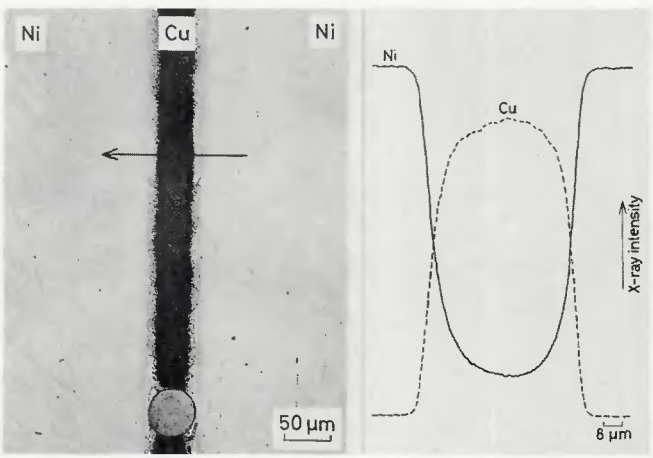

Fig. 4 — Microstructure and EPMA line analysis of Ni-8Cu-Ni joint at 50 µm (0.002 in.), brazed at 1125°C (2057°F) for 8 min

9. High carbon steel with 0.85% C.
10. High speed T4 tool steel with 18% W, 4% Cr, 1% V, 5% Co and 0.85% C.
11. Type 304 stainless steel with 18% Cr, 8% Ni and 0.05% C.

Pure 99.99% copper (Cu) was used as filler metal, and tungsten (W) wires having appropriate diameters were adapted for use as joint spacers.

With certain exceptions, all brazing was conducted in an argon atmosphere under a vacuum of 0.133 Pa (10^{-3} torr) as previously described in literature (Ref. 1). The exceptions were similar metal-to-metal joints involving Cr, W, and V.

After brazing, each specimen was sectioned perpendicularly to the brazed surface and examined metallographically. Also, electron probe microanalysis (EPMA) was conducted on specimen joints under the following conditions:

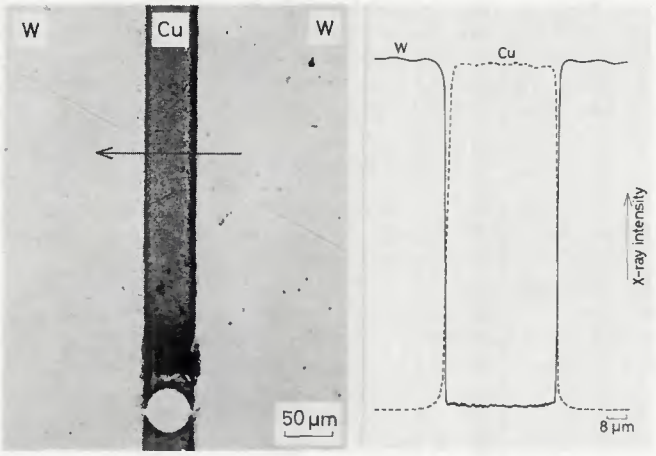

Fig. 5 — Microstructure and EPMA line analysis of W-8Cu-W joint at 50 µm (0.002 in.), brazed at 1125°C (2057°F) for 8 min in Ar

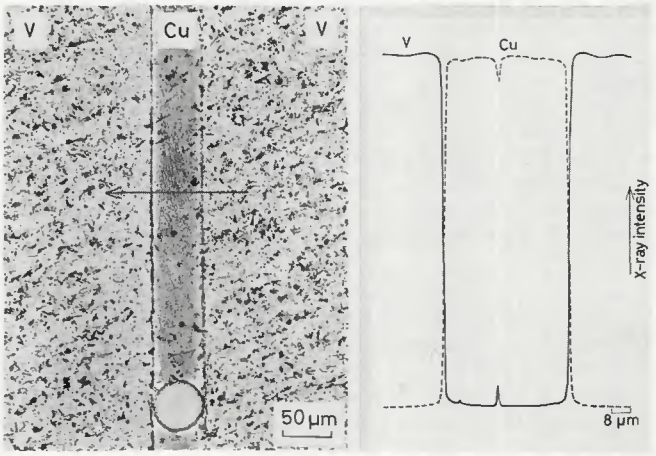

Fig. 6 — Microstructure and EPMA line analysis of V-8Cu-V joint at 50 µm (0.002 in.), brazed at 1125°C (2057°F) for 8 min in Ar

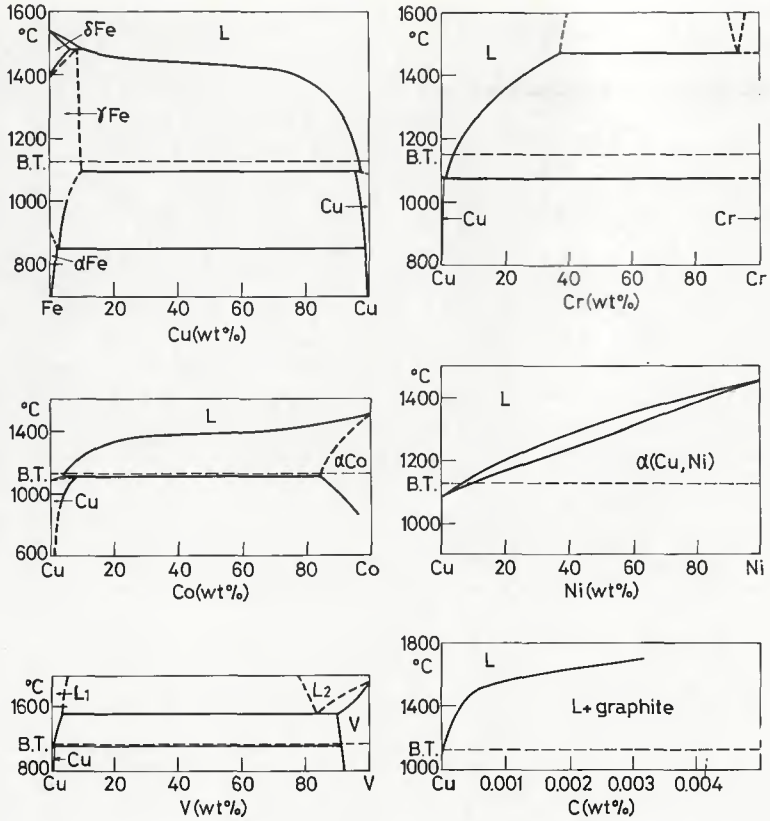

Fig. 7 — Cu-Fe, Cu-Cr, Cu-Co, Cu-Ni, Cu-V and Cu-C phase diagrams. BT — brazing temperature

voltage — 20 kV; current — 3.4 nA. The etchants were 2% nital, H_2O_2 (35%), Grard reagent (5g $FeCl_3$, 10ml HCl, 100ml H_2O), and a reagent consisting of 5g $FeCl_3$, 2ml HCl, and 100ml of ethanol. To check the mechanical properties of the brazed joint, each of a series of alloy steel C steel joints was submitted to shear tests (Ref. 1) after filing away the fillet.

Results and Discussion for Brazing of Similar Materials

Figures 1 to 6 illustrate the cross-section microstructures and EPMA line analyses of similar Fe, Cr, Co, Ni, W and V joints, brazed with Cu at 1125°C (2057°F) for 8 min. Because there was no wetting, it was impossible to braze C (graphite) with Cu filler metal.

In similar metal-to-metal joints, the base metal dissolves in molten Cu and, simultaneously, the molten Cu penetrates into the base metal. However, the dissolution of the base metal into molten Cu does not exceed its equilibrium quantity as illustrated in Fig. 7 (Ref. 6), no matter how long the heating time. Here the base metal boundary is saturated with Cu by the penetration of molten Cu.

Figure 8 shows the effect of heating time on Fe quantity dissolved in molten Cu for brazed low carbon steel to low carbon steel joints, measured by EPMA analysis (Ref. 7). The experimental data shows that, at 1125°C (2057°F), the amount of Fe dissolved in molten Cu is approximately 3%; this is nearly equal to that of the Fe-Cu phase diagram shown in Fig. 7, and the time to attain equilibrium is within 60 seconds. Bredzs and Schwartzbart (Ref. 8) have also reported that the molten Cu becomes saturated with Fe during the filling period of the capillary gap, or very shortly afterwards.

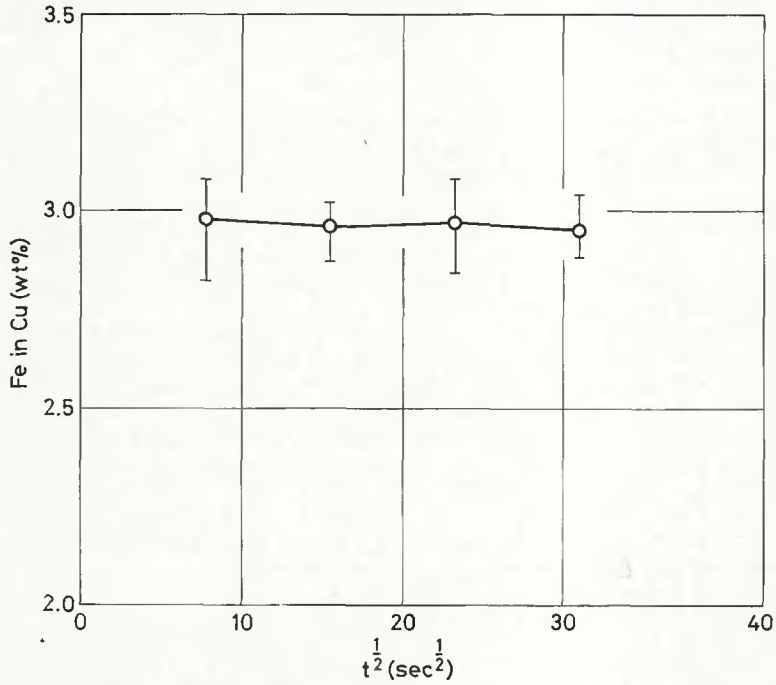

Fig. 8 — Effect of heating time on dissolution of steel into molten copper in similar 0.11% C steel joints at 50 μm (0.002 in.), brazed with copper at 1125°C (2057°F)

Brazing of Dissimilar Materials—Results and Discussion

Fe-Cr

Figure 9 illustrates the microstructures and EPMA line analyses for dissimilar Fe-Cr joints brazed at 1150°C (2102°F) for 2, 8 and 32 min.

In Fig. 9, it appears that the plate-like alloys, which contain the component of each opposite base metal, are deposited in both base metal braze interfaces. Here they grow into the base metal with heating time at a constant brazing temperature. At both base metal braze interfaces, these plate-like phases have the same composition: 26% Cr, 4% Cu and the balance Fe. During heating, these values were retained.

According to the Fe-Cr phase diagram in Fig. 10, two solid phases — γFe and (αFe, Cr) — exist at the 1150°C (2102°F) brazing temperature. Thus, any of the deposited phases shown in Fig. 9 can be considered as (αFe, Cr), containing a little Cu.

The oblique-section microstructure shown in Fig. 11 indicates that the streaks in the plate-like phase on Fe side are the grain braze interfaces. Furthermore, the thin white phase between Fe base metal and the plate-like phase is also recognized in Figs. 9 and 11. It must be γFe resulting from the penetration of Cr and

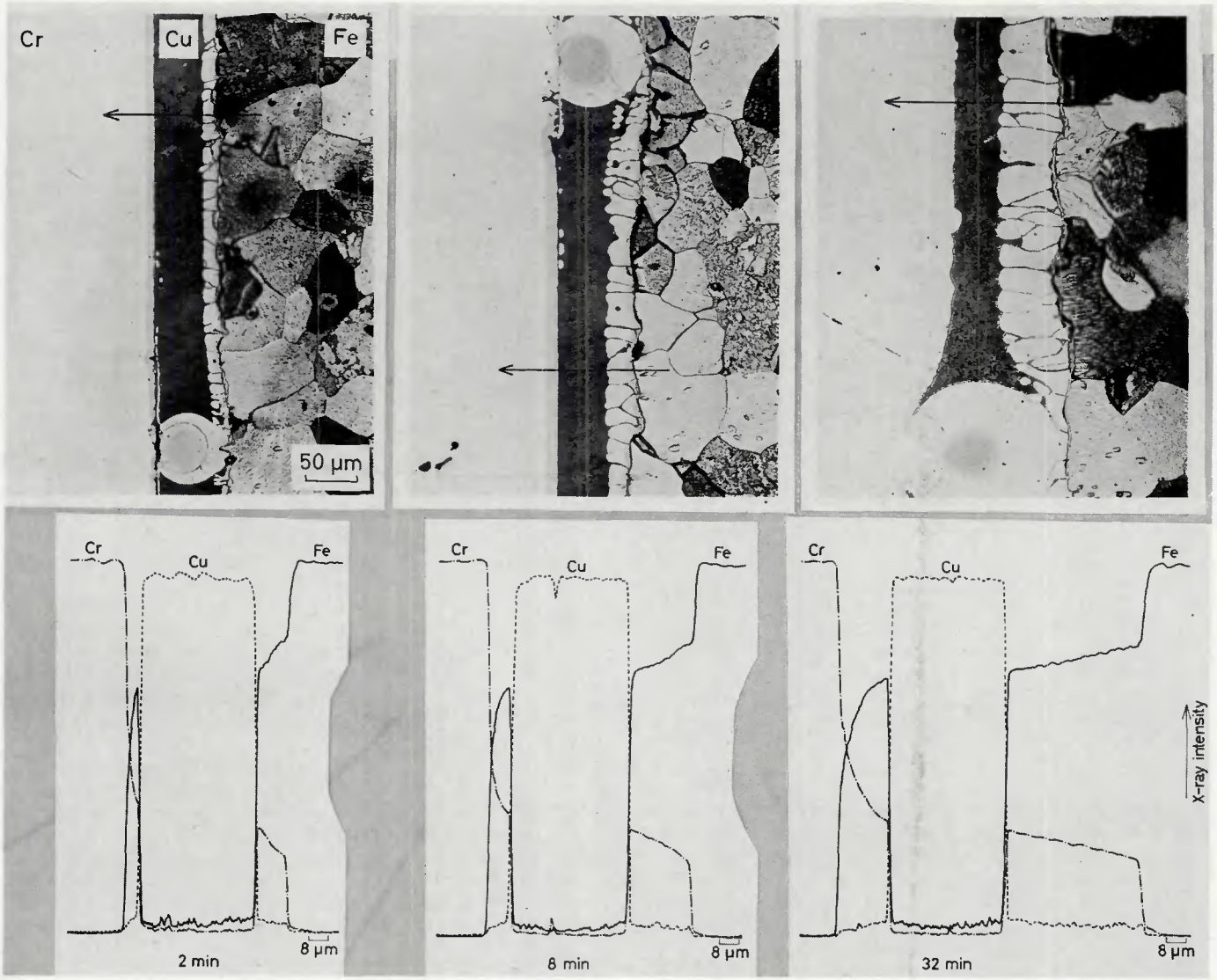

Fig. 9—Microstructure and EPMA line analysis of Fe-BCu-Cr joints at 50 μm (0.002 in.), brazed at 1150°C (2102°F) for 2, 8 and 32 min. ×200 (reduced 23% on reproduction)

Cu from the plate-like phase toward the Fe base metal, because this consists of 13 to 8% Cr, 4 to 3% Cu, and the balance Fe.

Fe-Co

Figure 12 illustrates the microstructure and EPMA line analysis of a Fe-Co joint; the plate-like phases including each opposite base metal component are deposited in both braze interfaces. The composition of both deposited phases is the same—that is, 44% Co, 42% Fe and 14% Cu, at both braze interfaces. These values do not vary with heating time, as previously mentioned for Fe-Cr.

According to the Fe-Co phase diagram in Fig. 10, only one solid phase (γFe, αCo) exists at brazing temperature. Therefore, both plate-like phases must be (γFe, αCo) and include Cu.

Fe-Ni

Figure 13 illustrates the microstructure and EPMA line analysis of a dissimilar Fe-Ni joint; the Fe-Ni-Cu alloys are deposited in both braze interfaces. Metallographically, the alloy on the Fe side in Fig. 13 can be seen as plate-like; however, that on the Ni side is hardly distinguished from both Ni base metal and Cu filler metal.

The compositions of both alloys at the braze interfaces are 46% Fe, 29% Cu and 25% Ni on the Fe side, and 58% Ni, 30% Cu and 12% Fe on Ni side. According to the Fe-Ni phase diagram in Fig. 10, only one solid phase γ(γFe, Ni) exists at the 1125°C (2057°F) brazing temperature. Thus, it can be concluded both deposited phases are γ(γFe, Ni) and contain a large amount of Cu.

Fe-W

Figure 14 illustrates the microstructure and EPMA line analysis of a dissimilar Fe-W joint. As a result of the change in the relative position of the filler metal-base metal interfaces and W spacer, it is evident in Fig. 14 that the Fe base metal dissolves in molten Cu and the plate-like alloy deposits from the W base metal.

The plate-like phase is composed of two layers—that is, the outer layer adjacent to the Cu filler metal consists of 10 to 9% Cu, 1 to 2% W and the rest Fe, the inner layer consists of 9 to 8% Cu, 3 to 9% W and the rest Fe. Furthermore, another plate-like white phase is observed between the inner layer and the W base metal. The relation between W spacer and the white phase, which consists of 30 to 28% Fe, 2 to 1% Cu and the rest W, indicates that this phase may be caused by the penetration of Fe and Cu from the deposited phase. As can be recognized in Fig. 14, 1 to 2% W also exists in both the Fe base metal boundary and the insular phase nearby that.

According to the Fe-W phase diagram shown in Fig. 10, γFe, αFe, Fe_7W_6 and W exist at the brazing temperature. More-

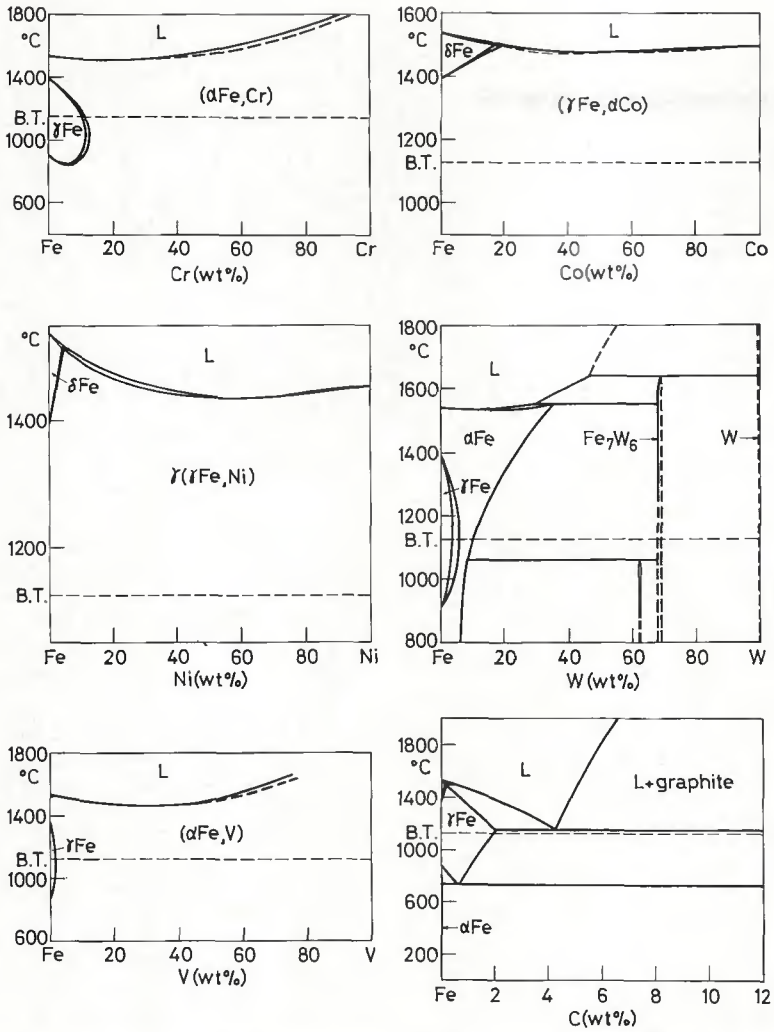

Fig. 10 — Fe-Cr, Fe-Co, Fe-Ni, Fe-W, Fe-V and Fe-C phase diagrams. BT — brazing temperature

over, the outer and inner layers of the plate-like phase are γFe(αFe at room temperature) and αFe, respectively, and include Cu; the white phase is the intermetallic compound (*i.e.*, Fe_7W_6), and contains only a little Cu. When a rough cut occurred at the Fe-W joint, cracking frequently occurred at the white layer-W base metal interface. On the other hand, both the Fe base metal braze interface and the insular phase are γFe(αFe at room temperature). Additional information concerning the Fe-W joint is available in the literature (Ref. 9).

Fe-V

Figure 15 illustrates the microstructure and EPMA line analysis of a dissimilar Fe-V joint; the Fe base metal dissolves into molten Cu and the plate-like alloy, which consists of 11 to 24% V, 4 to 3% Cu and the rest Fe, is deposited in the V base metal boundary. Also, the granular alloy containing V is found on the Fe side. This granular phase is composed of two parts. The higher V part consists of 11% V, 4% Cu and the rest Fe; the lower V part consists of 5 to 4% V, 5 to 4% Cu and the rest Fe.

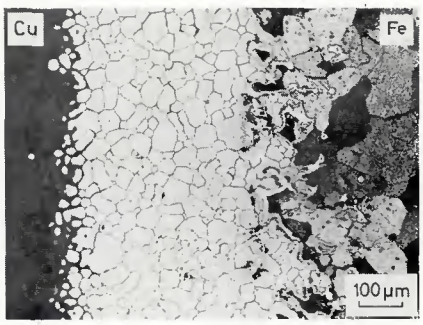

Fig. 11 — Oblique section of Fe-BCu-Cr joint at 100 μm (0.004 in.), brazed at 1150°C (2102°F) for 32 min

According to the Fe-V phase diagram in Fig. 10, two solid phases γFe and (αFe, V) exist at brazing temperature. Therefore, it can be concluded that the plate-like phase is (αFe, V) containing a small amount of Cu, whereas the granular phase is constituted of (αFe, V) and γFe that includes a small amount of Cu. Additionally, at the time of cutting the Fe-V joint, cracking often occurred at the plate-like phase/V base metal interface.

Fe-C

Figure 16 illustrates the microstructure and EPMA line analysis of a dissimilar Fe-C(graphite) joint. Since the graphite base metal has peeled off on cutting, the synthetic resin including a Cu powder for electric conductivity is seen on the graphite side.

In Fig. 16, it is clear that the Fe base metal dissolves in molten Cu and that the columnar alloy is deposited from the graphite boundary. This columnar phase consists of 12 to 10% Cu, approximately 1% C and the rest Fe, quite similar to that in dissimilar C steel joint (Ref. 1). According to the Cu-Fe and Fe-C phase dia-

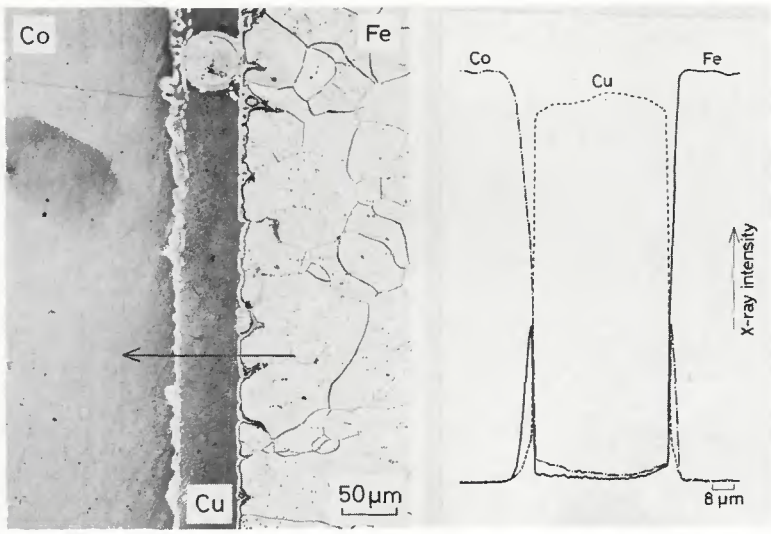

Fig. 12 — Microstructure and EPMA line analysis of Fe-BCu-Co joint at 50 μm (0.002 in.), brazed at 1125°C (2057°F) for 8 min

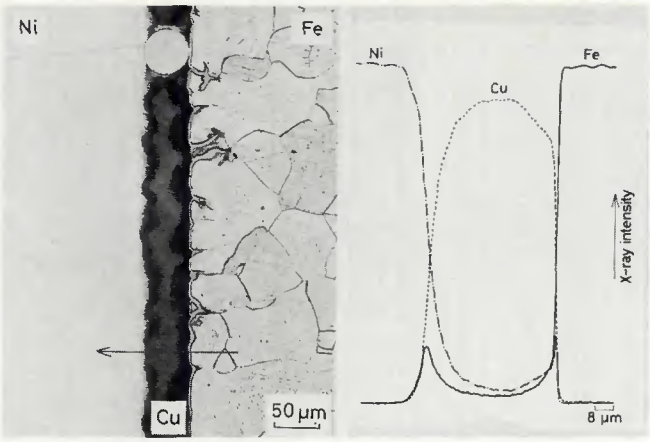

Fig. 13 — Microstructure and EPMA line analysis of Fe-BCu-Ni joint at 50 µm (0.002 in.), brazed at 1125°C (2057°F) for 8 min

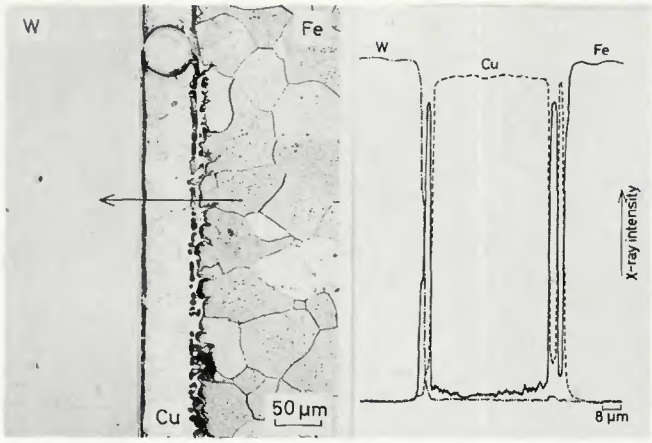

Fig. 14 — Microstructure and EPMA line analysis of Fe-BCu-W joint at 50 µm (0.002 in.), brazed at 1125°C (2057°F) for 8 min

grams, in Figs. 7 and 10, the columnar phase is γFe (pearlite at room temperature) and includes some Cu.

Space Model of A-B-C Phase Diagram

In the Cu brazing of Fe to Cr, Co, Ni, W, V and C, the dissolution and deposit of base metal occurs so that the alloy, which contains the component of the opposite base metal, develops in the brazing interface as has been shown. A discussion of the mechanism for this phenomenon follows.

According to the phase diagrams in Fig. 7, the equilibrium quantities of Fe, Cr, Co, Ni, V and C that dissolve in molten Cu at each brazing temperature are 3% Fe (4% Fe in the case of Fe-Cr), 4% Cr, 4% Co, 6% Ni, 0.3% V and approximately 0.0001% C (Ref. 10). It has been reported that W is insoluble in liquid Cu (Ref. 10). Nonetheless, it is possible to join W with Cu filler metal, as illustrated in Fig. 5; this means that W can be wet with molten Cu. From Fig. 5, the quantity of W in Cu was approximately 0.4% as determined by EPMA quantitative analysis. On the other hand, the solubilities of molten Cu in each base metal were 9% Cu in Fe, 16% Cu in Co, 91% Cu in Ni and 9% Cu in V, respectively, and nearly zero in Cr, W and C.

According to the diagrams in Fig. 10, at each brazing temperature the Fe base metal forms γFe and (αFe, Cr) in Fe-Cr; (γFe, αCo) in Fe-Co; γ(γFe, Ni) in Fe-Ni; γFe, αFe, Fe_7W_6 and W in Fe-W; γFe and (αFe, V) in Fe-V; γFe in Fe-C. In order to simplify discussion of the mechanism, one should consider a schematic model as illustrated in Fig. 17 that depicts the dissimilar brazing of base metals A and C with filler metal B at a temperature T. If we suppose that A, B, C and T are, respectively, Fe, Cu, Co and 1125°C (2057°F), the symbols a_0, c'_0, e_0 and e'_0 in Fig. 17 correspond to 3% Fe, 4% Co, 9% Cu and 16% Cu, respectively.

When the molten B flows into the clearance of both base metals A and C at the temperature T, the following occurs:

1. After a short time (Refs. 8, 11) at the A braze interface, base metal A dissolves in molten B up to its equilibrium quantity a_0 so that the liquid composition adjacent to the braze interface becomes $L_0(a_0, b_0, 0)$. Simultaneously, the molten B penetrates into the base metal A up to e_0 forming the solid phase $S_0(d_0, e_0, 0)$. On the other hand, at the C braze interface similarly to the A braze interface, the liquid phase becomes $L'_0(0, b'_0, c'_0)$ by the dissolution of the base metal C in molten B; at the same time, the solid phase $S'_0(0, e'_0, f'_0)$ is formed by the penetration of molten B into base metal C.

2. Because of a narrow joint clearance, the C component in molten B diffuses from the C braze interface to the A braze interface, where B is saturated with A; here C combines with component A to form the A-C alloy. We consider that the bonding force of A-C is significantly greater than those of A-B and B-C in a liquid B. During keeping A in B a_0, adding C to the liquid L_0 results in the change of liquid composition from L_0 to $L_1(a_0, b_1, c_1)$, as illustrated in Fig. 17. This is equivalent to the increase in temperature ΔT.

From the phase rule:

$$F = C^* - P + 2$$

where F = degrees of freedom,

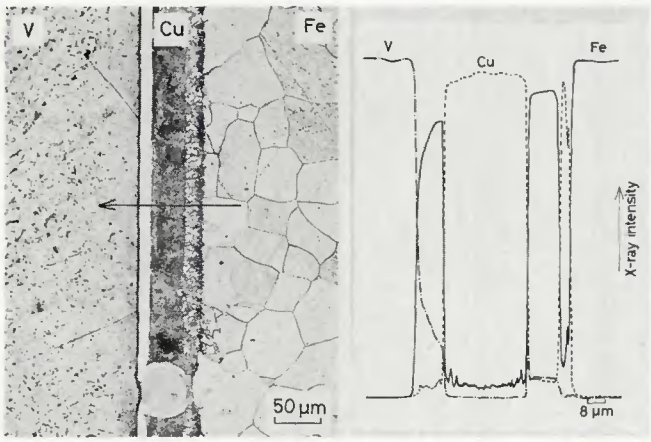

Fig. 15 — Microstructure and EPMA line analysis of Fe-BCu-V joint at 50 µm (0.002 in.), brazed at 1125°C (2057°F) for 2 min

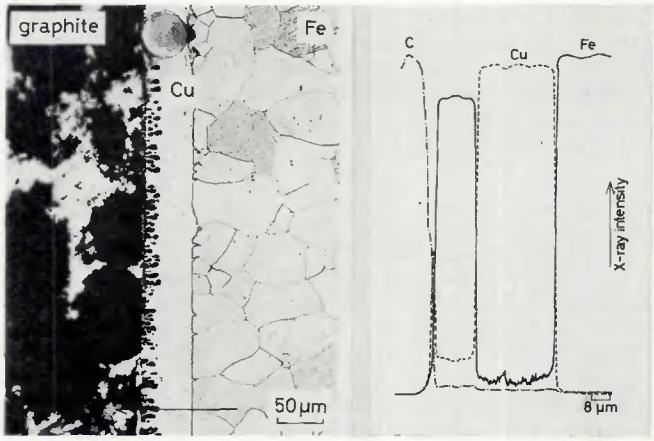

Fig. 16 — Microstructure and EPMA line analysis of Fe-BCu-graphite joint at 50 µm (0.002 in.), brazed at 1125°C (2057°F) for 1 min

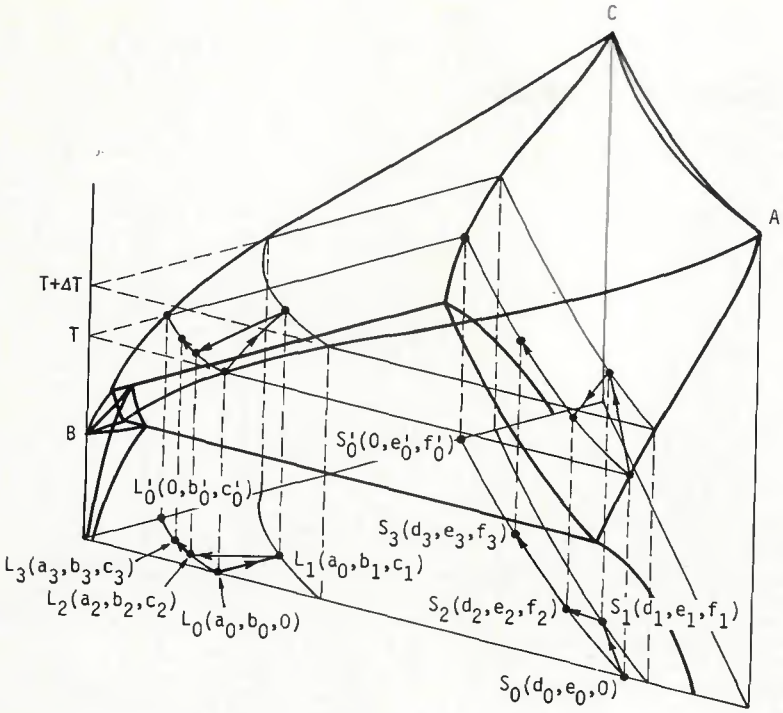

Fig. 17 — Space model of A-B-C phase diagram

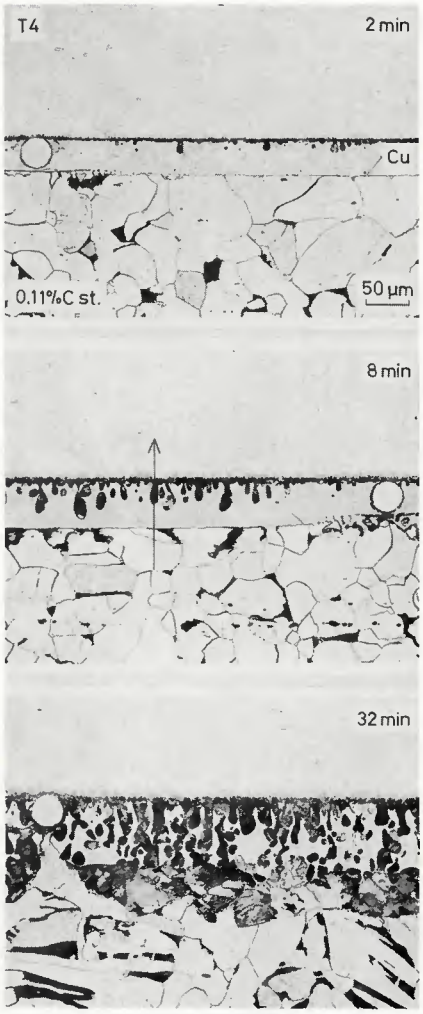

Fig. 18 — Microstructure of 0.11% C steel-BCu-T4 joints at 35 μm (0.0014 in.), brazed at 1125°C (2057°F) for 2, 8 and 32 min

C* = components in the system, and P = number of phases.

In a three-components system (C* = 3) containing two phases (P = 2) at equilibrium, F = C* − P + 2 = 3 − 2 + 2 = 3. If the pressure and the temperature are fixed, there is only one degree of freedom. Thus, when the liquid phase L_1 is fixed as previously discussed, the solid phase is determined automatically to be $S_1(d_1, e_1, f_1)$ as shown in Fig. 17.

3. Because the actual brazing temperature is kept at T, liquid L_1 can be regarded as a constitutional undercool even though there is no temperature gradient. Consequently, at the A braze interface the A-B-C solid solution corresponding to $S_2(d_2, e_2, f_2)$ is deposited in order to cancel the constitutional undercool. As a result, the liquid phase moves from L_1 to $L_2(a_2, b_2, c_2)$.

4. Since the C component, which has been supplied from the C braze interface, alloys ceaselessly with A in L_2 nearby the A boundary, C in L_2 increases so that the A-B-C solid solution includes higher C content deposits. In this manner, the liquid phase at the A braze interface moves along the L_0-L'_0 curve in Fig. 17. In doing so, it finally reaches the stable point $L_3(a_3, b_3, c_3)$. Also, the solid phase moves along the S_0-S'_0 curve and reaches $S_3(d_3, e_3, f_3)$ in equilibrium with the stable liquid phase L_3.

Since the C component of the deposited phase S_3 penetrates into the base metal A, the C content of S_3 decreases. Therefore, in order to recover the C content of S_3 to the previous level, the further C component in L_3 penetrates into S_3 from the L_3-S_3 interface. As a result, because the C concentration in L_3 decreases, the dissolution of the base metal C into L'_0 advances at the C boundary to maintain its equilibrium quantity. It is by such means that the deposited phase S_3 grows continuously after the liquid phase reaches its stable state L_3. As may be noted from Fig. 8, the time available for the molten B to reach its stable condition L_3 must be less than 60 seconds(s).

This mechanism also occurs in a similar way at the C braze interface. The liquid phase adjacent to the base metal C moves from L'_0 to L_3 along the L'_0-L_0 curve in Fig. 17, while the solid phase also moves from S'_0 to S_3 along the S'_0-S_0 curve. Thus, in the cases of Fe-Cr, Fe-Co and Fe-V where there is a solid solution throughout constituent, the composition of the deposited phase at both braze interfaces becomes the same as illustrated in Figs. 9, 12 and 15. However, in the case of Fe-Ni (this has a homogeneous solid solution), it is obvious from Fig. 13 that the B content of the deposited phase is considerably higher when compared with those in Fe-Cr, Fe-Co and Fe-V. According to the Cu-Ni phase diagram in Fig. 7, Ni can form a homogeneous solid solution with Cu as well as Fe, and contain a maximum of 91% Cu at the brazing temperature. Thus, the higher Cu content is probably caused by the fact that the bonding force of Ni-Cu in a liquid Cu is considerably larger compared to those of Fe-Cu, Cr-Cu, Co-Cu and V-Cu.

In the case of Fe-C, the deposited phase develops on only one base metal as illustrated in Fig. 16. The carbon (C) of graphite is insoluble in molten Cu, and Fe can only dissolve into molten Cu.

Dissimilar Alloy Steel Brazing

High Speed Tool Steel-Carbon Steel

Figure 18 illustrates the microstructures of high speed tool steel–low carbon steel joints at 35 μm (0.0014 in.), brazed at 1125°C (2057°F) for 2, 8 and 32 min. Also, Fig. 19 illustrates EPMA line analysis of the arrow in Fig. 18.

In Fig. 18, it is apparent that the low carbon steel dissolves into molten Cu and, simultaneously, the columnar alloy (similar to that in the dissimilar C steel joint) grows from the high speed tool steel with heating time and finally links

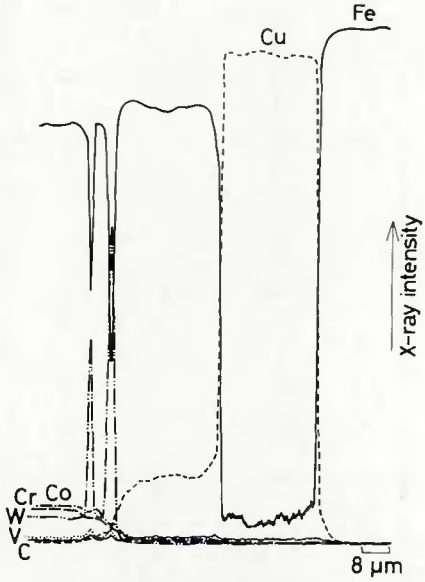

Fig. 19 — EPMA line analysis of 0.11% C steel-BCu-T4 joint, brazed at 1125°C (2057°F) for 8 min in Fig. 18

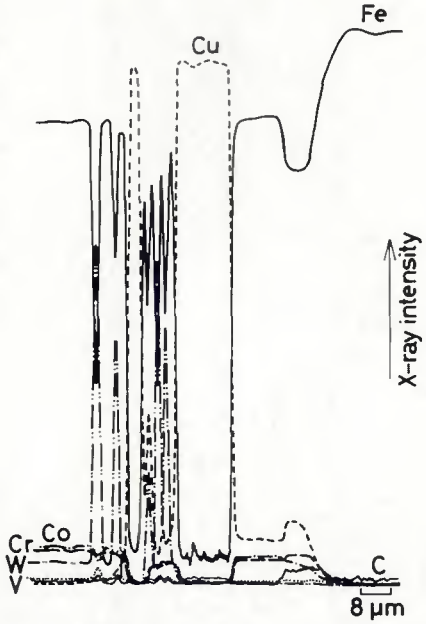

Fig. 21 — EPMA line analysis of 0.85% C steel-BCu-T4 joint, brazed at 1125°C (2057°F) for 8 min in Fig. 20

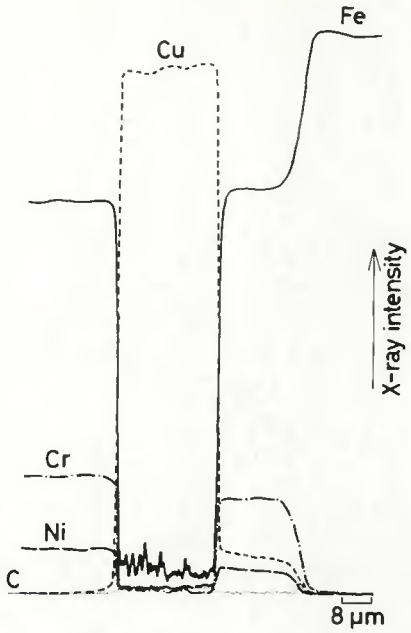

Fig. 23 — EPMA line analysis of 0.11% C steel-BCu-Type 304 stainless steel joint, brazed at 1125°C (2057°F) for 8 min in Fig. 22

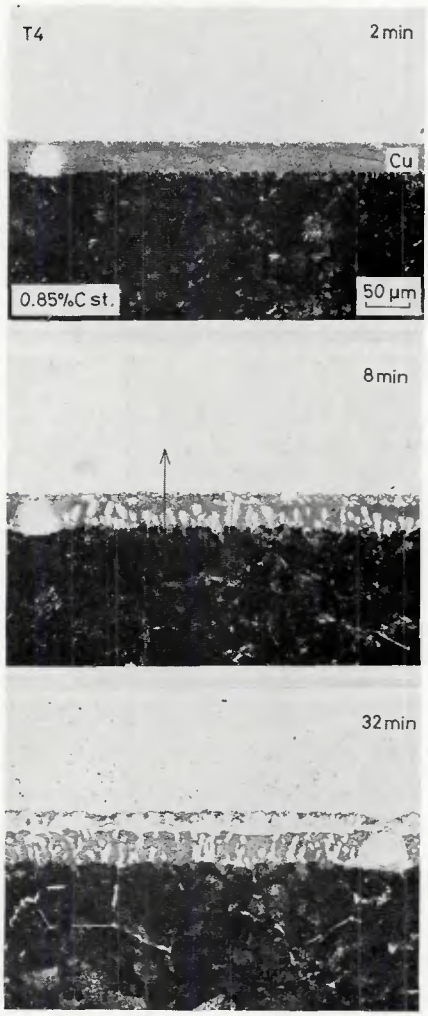

Fig. 20 — Microstructure of 0.85% C steel-BCu-T4 joints at 35 μm (0.0014 in.), brazed at 1125°C (2057°F) for 2, 8 and 32 min

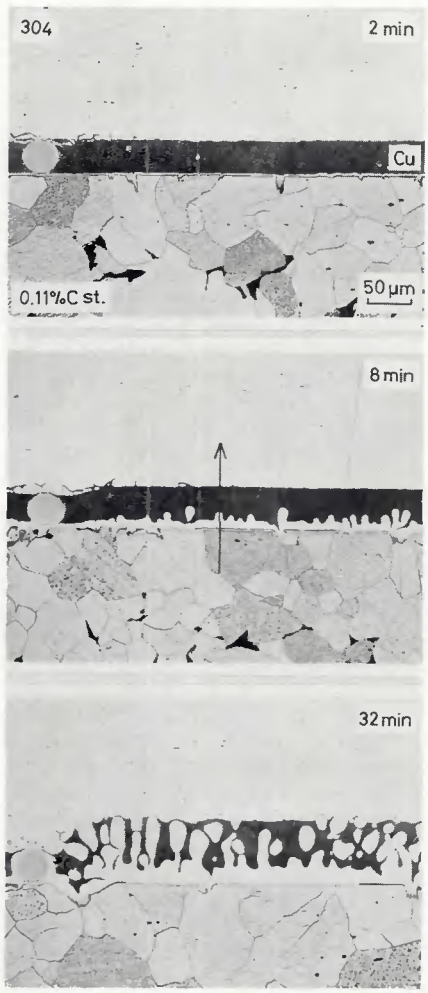

Fig. 22 — Microstructure of 0.11% C steel-BCu-Type 304 stainless steel joint at 35 μm (0.0014 in.), brazed at 1125°C (2057°F) for 2, 8 and 32 min

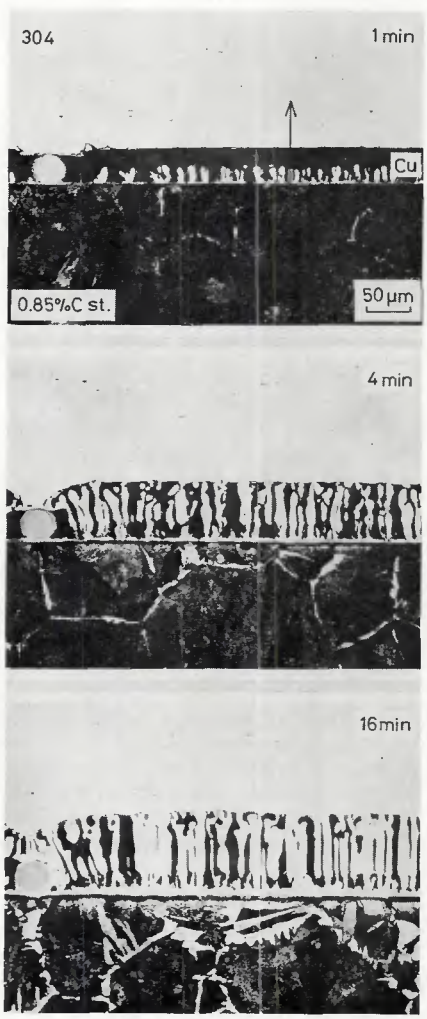

Fig. 24 — Microstructure of 0.85% C steel-BCu-Type 304 joints at 35 μm (0.0014 in.), brazed at 1125°C (2057°F) for 1, 4 and 16 min

both base metals. From Fig. 19, the columnar phase is the Fe-Cu-C-Co-Cr alloy consisting of 16 to 10% Cu, 0.6% C, 0.1 to 0.4% Co, 0.1 to 0.4% Cr and the rest Fe, without W and V. On the other hand, Figs. 20 and 21 illustrate the microstructures and EPMA line analysis of high speed tool steel-high carbon steel joints.

At first glance, the character of the microstructures in Fig. 20 is in sharp contrast with previous example. The high speed tool steel dissolves in molten Cu and, simultaneously, the columnar alloy grows increasingly from the high carbon steel. Apparently, this columnar phase is the Fe-Cu-Cr-Co-C-W-V alloy composed of two parts—that is, the white part consists of 9% Cu, 4% Co, 3% Cr, 0.7% W, 0.4% C, 0.3% V and the rest Fe, and the black part consists of 12 to 10% Cu, 4% Cr, 4 to 2% Co, 2 to 3% C, 0.4% V, 0.4% W and the rest Fe. Further, the decarburization can be observed in the high carbon steel, when the heating time is long. Because only the matrix of the high speed tool steel dissolves into molten Cu, the undissolved carbides are left in its boundary. However, the undissolved carbides are eventually surrounded by the deposited white phase, identical to the white part of the columnar phase—Fig. 20.

Since alloying elements such as W, Cr, V and C, except for Co in the high speed tool steel, are mainly included in the M_6C, $M_{23}C_6$ and MC carbides as an annealed condition, the concentration of those elements in its matrix is relatively low. However, during heating at 1125°C (2057°F), these carbides decompose so that the alloying element in the matrix increases. From EPMA analysis, the composition of the matrix after brazing was 6% W, 5% Co, 4% Cr, 0.6% V, 0.4% C and the rest Fe; this composition was almost equal to that measured by electrolytic isolation (Ref. 12). It became evident that, when the C content of the carbon steel to be combined would be lower than 0.4% C, the columnar phase was deposited from the high speed tool steel as shown in Fig. 18. With higher carbon steel, the high speed tool steel dissolved in molten Cu, leaving the carbides as shown in Fig. 20.

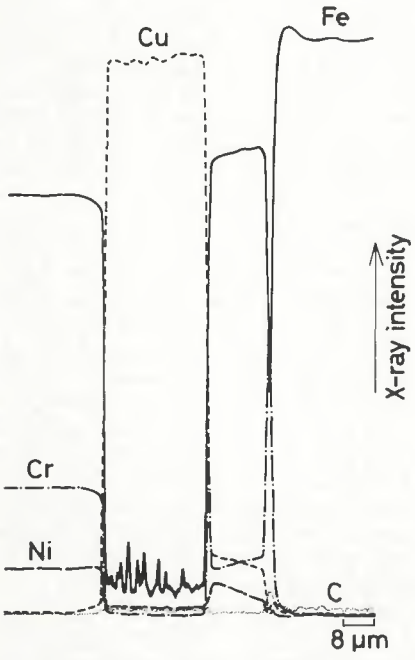

Fig. 25—EPMA line analysis of 0.85% C steel-BCu-Type 304 stainless steel joint, brazed at 1125°C (2057°F) for 1 min in Fig. 24

Stainless Steel-Carbon Steel

Figures 22 and 23 illustrate the microstructures and EPMA line analysis of stainless steel-low C steel joints; the stainless steel dissolves in molten Cu and, simultaneously, the columnar alloy grows from the low carbon steel, in which decarburization can be recognized. Due to the extremely small 0.05% C content of the stainless steel, the low carbon steel (0.11% C) can be regarded as on the higher C side. As evident from Fig. 23, the columnar phase consists of 13% Cr, 8 to 7% Cu, 5 to 4% Ni, 0.2% C and the rest Fe. However, a somewhat high carbon content was also recognized at the columnar phase-low C steel braze interface.

Figures 24 and 25 illustrate the microstructures and EPMA line analysis of stainless steel-high C steel joints; the stainless steel dissolves in molten Cu and, simultaneously, the columnar alloy grows rapidly from the high carbon steel, due to the large difference of C content between both base metals.

Remarkable decarburization can be seen in the high carbon steel. From Fig. 25, this columnar phase consists of 10 to 8% Cu, 6 to 7% Cr, 6 to 3% Ni, 0.3% C and the rest Fe. Using x-ray diffraction test for the sheared brazing surface of the specimen, it has been confirmed that the high Cr part at the columnar phase-high carbon steel braze interface in Fig. 25 consisted of the Cr carbides: $M_{23}C_6$ and M_7C_3. Further, at the skin of the columnar phase, the high Cr part, which might be considered to be chromium carbide, was often observed.

Figure 26 illustrates the stainless steel-Fe joint, where the difference of C content between both base metals becomes extremely small, *i.e.*, 0.037% C. Obviously, instead of the columnar phase in Fig. 22 where the difference of C content is 0.06% C, the plate-like alloy similar to that of Fe-Co joint shown in Fig. 12 is deposited in the Fe boundary. The stainless steel braze interface lacks both nickel and chromium; this may result in the significant loss of the chemical properties of the joint. The composition of both base metals at each braze interface becomes the same: 8% Cu, 6% Cr, 2% Ni and the rest Fe. It seems certain that the critical value for the difference in C content, which controls the configuration of the dissolution and deposit of base metal, exists between 0.037 and 0.06% C in the case of the Type 304 stainless steel-carbon steel joint.

Summarizing the data, one may conclude that, for alloy steel-carbon steel brazing, the C content of the base metal exerts the greatest influence on the dissolution and deposit, regardless of other alloying elements. Based on the Fig. 10 phase diagrams, the alloying elements such as Cr, Co, Ni, W, V and C, form a solid solution γFe with Fe at the brazing temperature. However, only C is intersti-

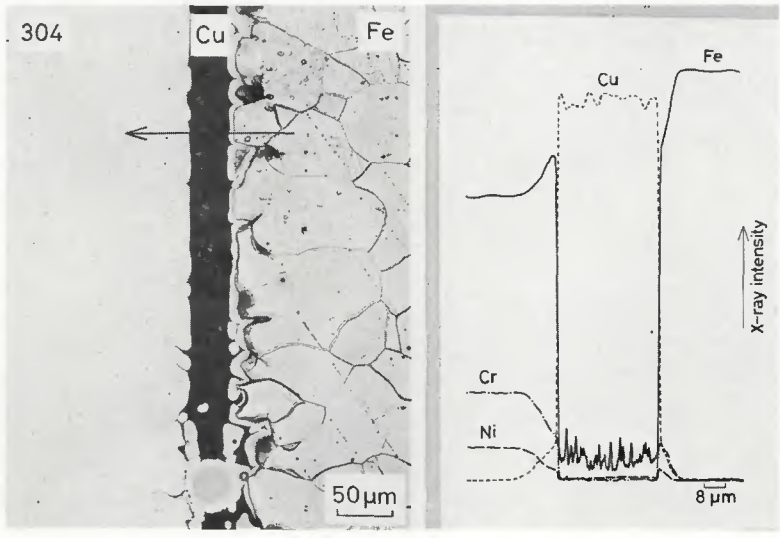

Fig. 26—Microstructure and EPMA line analysis of Fe-BCu-Type 304 stainless steel joint at 35 μm (0.0014 in.), brazed at 1125°C (2057°F) for 32 min

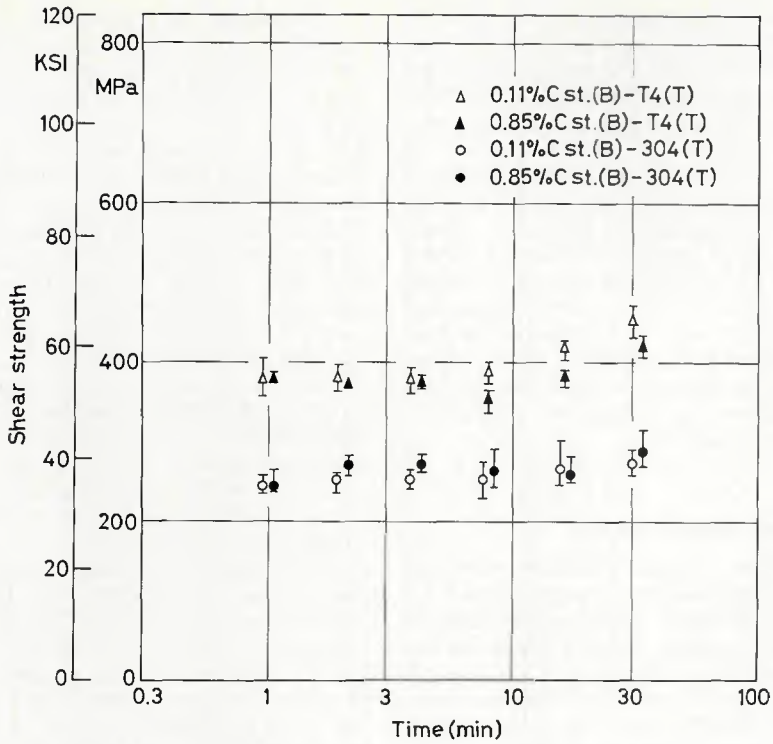

Fig. 27 — Effect of heating time on shear strength in dissimilar alloy steel joints at 35 μm (0.0014 in.), brazed at 1125°C (2057°F). B and T — base metal and tips in shear test, respectively

tial, but the others are substitutional. Also the 1125°C (2057°F) or 1150°C (2102°F) brazing temperature are only 42°C (76°F) or 67°C (121°F) above the 1083°C (1981°F) melting point of Cu. In general, a liquid metal retains the characteristics of the solid structure in the neighborhood of its melting point (Ref. 13). Therefore, it is assumed that, since molten Cu retains characteristics of its solid structure (a f.c.c. structure) at the brazing temperature, a solid solution γFe (a f.c.c. structure) does not enter into molten Cu as a disjointed atom, but as a massive (Ref. 14) associated compound (Ref. 15) due to a strong interaction between atoms (Ref. 16).

In view of the data, it seems logical to suggest that a low C iron alloy associated compound dissolved in molten Cu from the lower C base metal easily draws in C atoms, from the higher C base metal to form a high C iron alloy associated compound, due to:

1. The significantly greater bonding force of Fe-C compared to other alloying elements.
2. The ease with which a C atom can enter the γFe associated compound owing to its being an interstitial type.
3. The fast migration of C atoms through the higher C base metal to the braze interface because of the rapid diffusion rate.

Thus, the concentration of the high C iron associated compound in molten Cu adjacent to the higher C base metal rapidly exceeds its equilibrium quantity so that, because of a constant brazing temperature, a "constitutional supercooling" takes place; the excess component is deposited as the columnar alloy in the same manner as the dissimilar C steel brazing (Ref. 1).

The significant conclusion to be drawn from this study is that the dissolution and deposit of base metal in dissimilar alloy steel brazing is most severely affected by the difference of C content between both base metals, regardless of other conventional alloying elements.

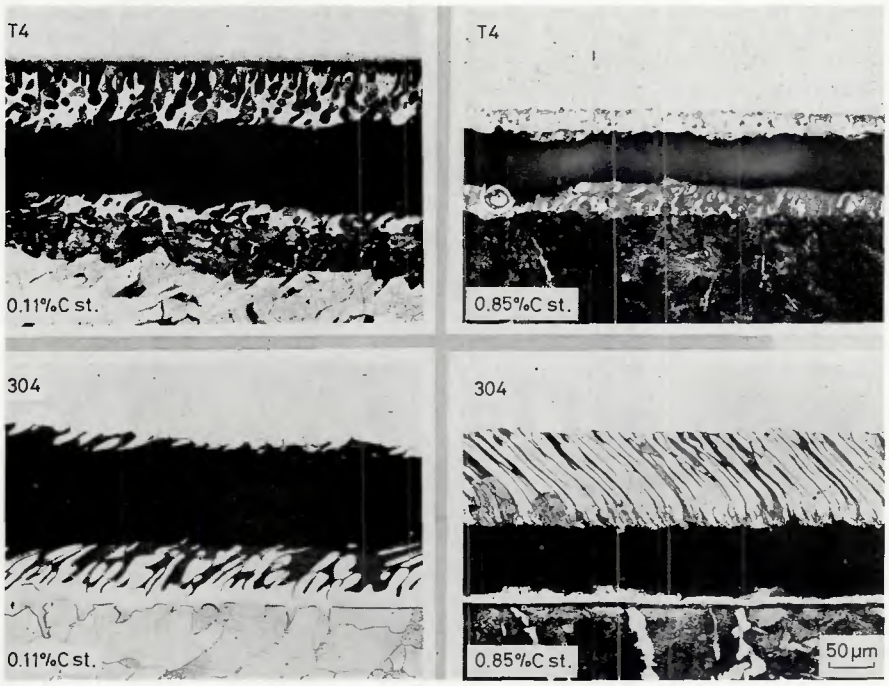

Fig. 28 — Microstructures of sheared dissimilar alloy steel joints at 35 μm (0.0014 in.), brazed at 1125°C (2057°F) for 32 min. ×200 (reduced 41% on reproduction)

Shear Strength

Figure 27 illustrates the results of the shear tests for dissimilar alloy steel joints as already shown in Figs. 18, 20, 22 and 24. Figure 28 illustrates cross-section microstructures after shear testing.

In the case of the high speed tool steel-low carbon steel joint, the joint sheared in the Cu layer, and its shear strength was about 382 MPa (55 ksi). However, after linking both base metals with the deposited columnar phase, shearing occurred across the phase as shown in Fig. 28, so that its shear strength increased to 451 MPa (65 ksi). Also in the case of high speed tool steel-high C steel joint, the shearing always occurred at the Cu layer-undissolved carbide interface shown in Fig. 28, regardless of heating time. But, its shear strength increased from about 373 MPa (54 ksi) to 422 MPa (61 ksi) with heating time. This presumably was caused by strengthening of the Cu-carbide interface due to the deposit of the alloy around the undissolved carbides.

In the case of the stainless steel-low carbon steel joint, the shear strength of the joint slightly increased from about 255 MPa (37 ksi) to 275 MPa (40 ksi) as a result of the linking of both base metals

with the columnar phase—Fig. 28. Also, in the case of stainless steel-high carbon steel joint, the joint sheared in the Cu layer before both base metals were linked with the columnar phase; its shear strength was 245 MPa (36 ksi). After linking, the shearing always occurred at the Cr carbide layer formed at the high carbon steel braze interface as shown in Fig. 28.

When the joint sheared in the Cu layer, shear strength in the case of the high speed tool steel was considerably higher than that in the case of the stainless steel. This might have been caused by the difference of hardness between high speed tool steel and stainless steel as a tip in shear test.

Figure 29 illustrates the effect of joint clearance on shear strength in dissimilar alloy steel joints; results obtained with the similar carbon steel joint are included for comparison. Figure 30 illustrates the microstructures of specimens sheared at 0* μm(0* in.) joint clearances. In Fig. 29, it is particularly evident that the narrower the joint clearance, the higher is the shear strength of the joint. However, the degree of this effect is more remarkable for the dissimilar metal joints compared to similar metal joints.

In the high speed tool steel-high carbon steel joint with 0* μm(0* in.) joint clearance†, shearing occurred in the high carbon steel base metal as shown in Fig. 30; its shear strength advanced to 618 MPa (90 ksi). Also, shearing of the carbon steel base metal in place of the brazed part occurred in both alloy steels-low carbon steel joints with 0* μm(0* in.) clearance as shown in Fig. 30. In Fig. 29, however, the shear strength for high speed tool steel is somewhat higher than that for the stainless steel. This may result from both the difference of hardness between both alloy steels and also the complete decarburization of the low carbon steel base metal in the latter case. Because the rupture pattern in stainless steel-high C steel joint did not change with decreasing joint clearance, shear strength increased slightly even at 0* μm(0* in.) clearance compared to above examples. Further, in the similar carbon steel joints, shearing always occurred in the Cu layer regardless of joint clearance.

†0* denotes press fit (no spacer).

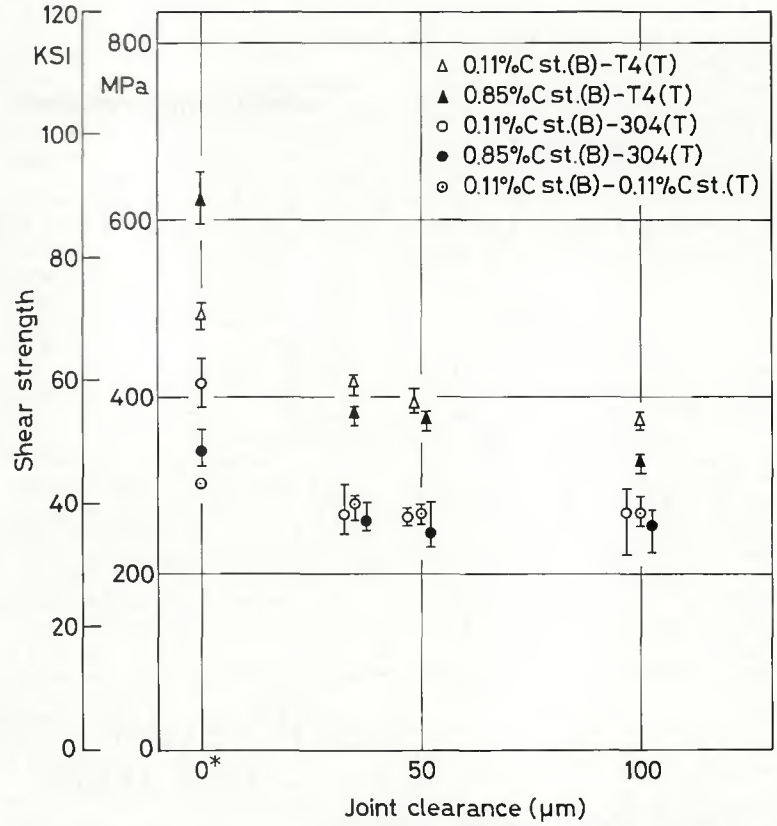

Fig. 29—Effect of joint clearance on shear strength in dissimilar alloy steel joints, brazed at 1125°C (2057°F) for 16 min. Asterisk (*) indicates press fit

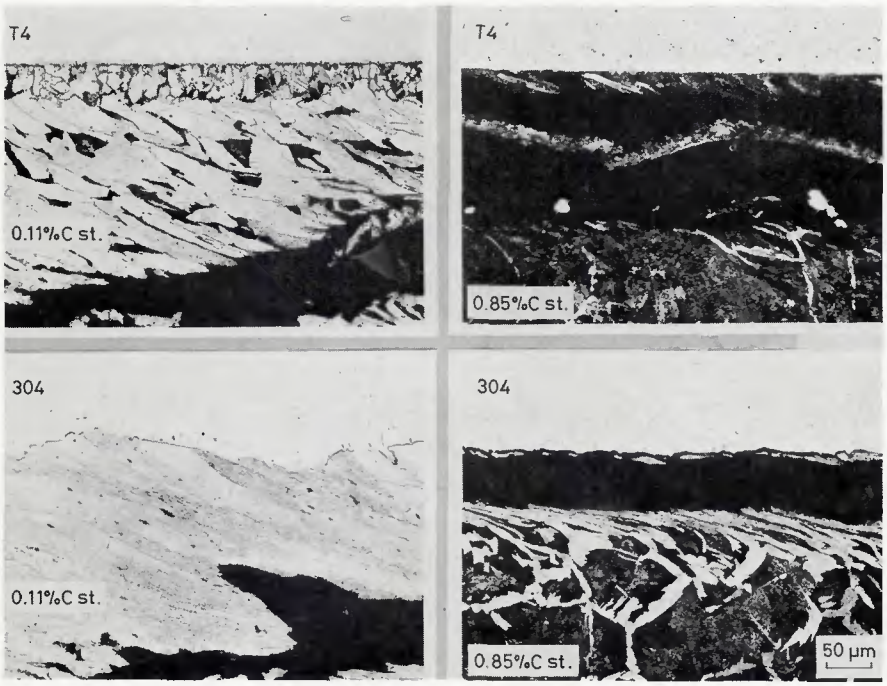

Fig. 30—Microstructures of sheared dissimilar alloy steel joints at 0 μm (0* in.), brazed at 1125°C (2057°F) for 16 min. Asterisk (*) indicates press fit. ×200 (reduced 41% on reproduction)*

Conclusions

1. In joining Fe with Cu filler metal to alloying elements such as Cr, Co, Ni, W, V and C commonly found in steel, a "dissolution and deposition of base metal" occurs. As a result, an alloy that includes the component of the opposite base metal develops in the braze interface at a constant brazing temperature.

2. Of the alloying elements, carbon (C) exerts the greatest influence on the dissolution and deposition of base metal.

3. When the alloy steels, such as high speed tool steel and stainless steel, containing alloying elements are brazed to both high and low carbon steels with Cu filler metal, more of the lower C base metal (compared to the higher C base metal) dissolves in molten Cu and, simul-

taneously, higher C base metal is deposited in the columnar alloy regardless of other alloying elements.

4. The shear strength of dissimilar alloy steel-carbon steel joints is enhanced noticeably by linking both base metals with the deposited columnar phase. An exception occurs with stainless steel-high carbon steel joints when chromium carbides form at the high carbon steel braze interfaces.

References

1. Yoshida, T., and Ohmura, H. 1980. Dissolution and deposit of base metal in dissimilar carbon steel brazing. *Welding Journal* 59(10): 278-s to 282-s.

2. Yoshida, T., and Takigami, N. 1973. Brazing of metals: 18-21. Symposium in Japan Inst. of Metals (in Japanese).

3. Yoshida, T., and Ohmura, H. 1980. Dissolution and deposit of base metal in brazing to dissimilar materials and its application (part 3), copper brazing to iron and molybdenum or tungsten. *Journal of Japan Welding Society* 49(2): 117-123 (in Japanese).

4. Ohmura, H., and Yoshida, T. 1981. Dissolution and deposit of base metal in brazing to dissimilar materials and its application (part 4), copper brazing of iron to chromium, cobalt and nickel. *Journal of Japan Welding Society* 50(9): 924-930 (in Japanese).

5. Ohmura, H., and Yoshida, T. 1982. Dissolution and deposit of base metal in brazing to dissimilar materials and its application (part 5), copper brazing to alloy steel and carbon steel. *Journal of Japan Welding Society* 51(5): 410-416 (in Japanese).

6. Lyman, T. 1973. Metals handbook, 8. American Society for Metals.

7. Toyota Central R&D Lab., Inc. 1970. Diagrams and tables for quantitative electron probe microanalysis.

8. Bredzs, N., and Schwartzbart, H. 1958. Metallurgy of bonding in brazed joints. *Welding Journal* 37(11): 493-s to 498-s.

9. Yoshida, T., and Ohmura, H. 1982. Effect of nickel plating on Fe-BCu-Mo and -W. *Welding Journal* 61(11): 363-s to 372-s.

10. Hansen, M. 1958. *Constitution of binary alloys*. New York: McGraw-Hill.

11. Ishida, T. 1970. The brazing reaction of iron base metal with copper (report 1), on the dissolution of iron base metal in molten copper. *Journal of Japan Welding Society* 39(4): 259-268 (in Japanese).

12. Sato, T., Nishizawa, T., and Murai, K. 1959. On carbides in tungsten high speed steels. *Journal of the Iron and Steel Inst. of Japan* 45(4): 409-415 (in Japanese).

13. Waseda, Y., Tokuda, M., and Ohtani, M. 1975. The structure of molten Fe and Fe-C alloys by X-ray diffraction. *Journal of the Iron and Steel Inst. of Japan* 61(1): 54-70 (in Japanese).

14. Prigogine, I., and Defay, R. 1950. *Thermodynamique chimique*. Éditions Desoer, Liége.

15. Wasai, K., and Mukai, K. 1981. Application of the ideal associated solution model on description of thermodynamic properties of several binary alloys. *Journal of Japan Inst. of Metals* 45(6): 593-602 (in Japanese).

16. Ohmura, H., and Yoshida, T. 1980. Mechanism of deposit to columnar iron in dissimilar carbon steel brazing. Preprints of national meeting of J.W.S., no. 27: 58-59 (in Japanese).

WRC Bulletin 293
April 1984

Current Welding Research Problems
Compiled and edited by R. A. Kelsey, G. W. Oyler and C. R. Felmley, Jr.

This listing of current welding research problems was published to assist universities, industrial and research organizations and government agencies, by pointing out the welding problems requiring solution or additional study. These submittals were provided to the Welding Research Council University Research Committee by members of the WRC Project Committees, the attendees at the Conference on the National Needs in Welding Technology, April 28, 1983, and the participants at the ONR Welding Science Workshop on March 24-25, 1983.

Publication of this listing of welding research problems was sponsored by the University Research Committee of the Welding Research Council. The price of WRC Bulletin 293 is $15.00 per copy, plus $5.00 for postage and handling. Orders should be sent with payment to the Welding Research Council, Room 1301, 345 E. 47 St., New York, NY 10017.

WRC Bulletin 298
September 1984

Long-Range Plan for Pressure-Vessel Research—Seventh Edition
By the Pressure Vessel Research Committee

Every three years, the PVRC Long-Range Plan is up-dated. The Sixth Edition was widely distributed for review and comment. Up-dated problem areas have been suggested by ASME, API, EPRI and other organizations. Most of the problems in the Sixth Edition have been modified to meet current needs, and a number of new problems have been added to this Seventh Edition.

The list of "PVRC Research Problems" is comprised of 58 research topics, divided into three groups relating to the three divisions of PVRC; i.e., materials, design and fabrication. Each project is outlined briefly in a project description, giving the title, statement of problem and objectives, current status and action proposed.

Because of budget limitations, PVRC will not be able to investigate all of these problems in the foreseeable future. Therefore, the cooperation and efforts of other groups in studying these areas is invited. If work is planned on one of the problems, PVRC should be informed in order to avoid duplication.

Publication of this bulletin was sponsored by the Pressure Vessel Research Committee of the Welding Research Council. The price of WRC Bulletin 298 is $13.50 per copy, plus $5.00 for postage and handling. Orders should be sent with payment to the Welding Research Council, Room 1301, 345 E. 47th St., New York, NY 10017.